Cell Reports
Report

Competition between NBS1 and ATMIN Controls ATM Signaling Pathway Choice

Tianyi Zhang,[1,4] Kay Penicud,[1,4] Christopher Bruhn,[2] Joanna I. Loizou,[1] Nnennaya Kanu,[1] Zhao-Qi Wang,[2,3] and Axel Behrens[1,*]

[1]Mammalian Genetics Laboratory, Cancer Research UK, London Research Institute, 44 Lincoln's Inn Fields, London WC2A 3LY, UK
[2]Leibniz Institute for Age Research, Fritz Lipmann Institute, Beutenbergstrasse 11, 07745 Jena, Germany
[3]Faculty of Biology and Pharmacy, Friedrich Schiller University, Fuerstengraben 26, 07743 Jena, Germany
[4]These authors contributed equally to this work
*Correspondence: axel.behrens@cancer.org.uk
http://dx.doi.org/10.1016/j.celrep.2012.11.002

SUMMARY

Ataxia telangiectasia mutated (ATM) protein kinase activation by DNA double-strand breaks (DSBs) requires the Mre11-Rad50-NBS1 (MRN) complex, whereas ATM interactor (ATMIN) protein is required for ATM signaling induced by changes in chromatin structure. We show here that NBS1 and ATMIN proteins compete for ATM binding and that this mechanism controls ATM function. DSB-induced ATM substrate phosphorylation was increased in *atmin* mutant cells. Conversely, NBS1 deficiency resulted in increased ATMIN-dependent ATM signaling. Thus, the absence of one cofactor increased flux through the alternative pathway. Notably, ATMIN deficiency rescued the cellular lethality of NBS1-deficient cells, and NBS1/ATMIN double deficiency resulted in complete abrogation of ATM signaling and profound radiosensitivity. Hence, ATMIN and NBS1 mediate all ATM signaling by DSBs, and increased ATMIN-dependent ATM signaling explains the different phenotypes of *nbs1*- and *atm*-mutant cells. Thus, the antagonism and redundancy of ATMIN and NBS1 constitute a crucial regulatory mechanism for ATM signaling and function.

INTRODUCTION

Ataxia telangiectasia mutated (ATM), the protein kinase that is mutated in patients with ataxia telangiectasia, is a master regulator of the cellular response to DNA damage (Derheimer and Kastan, 2010; Lee and Paull, 2007; Lukas et al., 2011; McKinnon, 2004; Savitsky et al., 1995). ATM is activated by two main cofactors, Mre11-Rad50-NBS1 (MRN) and ATM interactor (ATMIN), in a stimulus-dependent manner (Kanu and Behrens, 2008). The MRN complex is required for ATM activation by double-strand breaks (DSBs; Lee and Paull, 2007; Uziel et al., 2003), whereas ATM signaling triggered by changes in chromatin structure requires ATMIN (Kanu and Behrens, 2007; Kanu et al., 2010; Loizou et al., 2011). However, the mechanism that instructs ATM to enter either the MRN-dependent or ATMIN-dependent signaling pathway is not well understood.

RESULTS AND DISCUSSION

Loss of ATMIN Enhances Canonical Ionizing-Radiation-Induced ATM Signaling

To investigate the mechanistic basis for ATM pathway selectivity, we analyzed ATM signaling in response to ionizing radiation (IR) in ATMIN-deficient mouse embryonic fibroblasts (*atmin*Δ/Δ MEFs; Kanu and Behrens, 2007; Figure S1A). Treatment with low doses of IR (0.8 Gy) resulted in modest ATM activation and substrate phosphorylation in control cells, but ATM signaling in *atmin*Δ/Δ MEFs, as judged by the levels of SMC1 and Kap1 phosphorylation (pSMC1 and pKap1), was considerably higher (Figure 1A). Immunofluorescence (IF) analysis revealed increased recruitment of active ATM phosphorylated at serine 1981 (pATM) and NBS1 to IR-induced foci (Figure 1B). We observed a notable difference in pATM average focus intensity, which was significantly increased in ATMIN-depleted cells over a time course ranging from 30 min to 24 hr (Figure 1C), whereas pATM focus area and the average number of foci were only marginally altered (Figures S1B and S1C).

To further analyze ATMIN function in response to IR in vivo, we generated mice lacking ATMIN in the intestine, a major radiosensitive organ in the body. Upon tamoxifen injection, the gut-specific *Villin-creERT* transgene (el Marjou et al., 2004) mediated efficient recombination of *atmin*F in the intestinal epithelium, resulting in a substantial decrease in ATMIN protein levels (Figure S1D). Tamoxifen-treated *atmin*F/F; *Villin-creERT* mice (*atmin*ΔG/ΔG mice) were healthy and their intestinal histology was unaltered compared with control animals (Figures S1E–S1H). Western blot analysis after whole-body irradiation corroborated that ATM substrate phosphorylation was increased in *atmin*ΔG/ΔG mice (Figure 1D). Moreover, the absence of ATMIN led to increased formation of 53BP1 foci (Figures 1E and 1F). Thus, the flux through the canonical IR-induced, NBS1-dependent arm of ATM signaling is increased in the absence of ATMIN.

ATMIN Competes with NBS1 for ATM Binding

NBS1 interacts directly with ATM, and a short C-terminal motif in NBS1 has been shown to contribute significantly to ATM/NBS1 binding (Falck et al., 2005). ATMIN interacts with ATM using

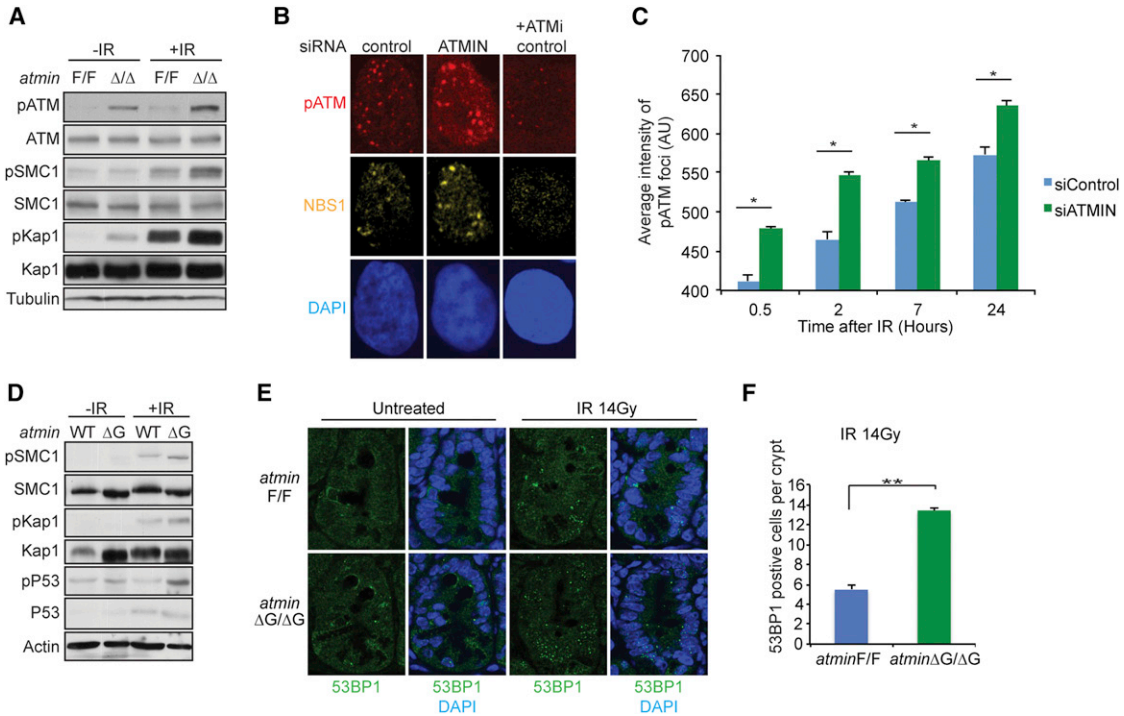

Figure 1. Loss of ATMIN Enhances Canonical IR-Induced ATM Signaling

(A) *atmin*F/F and Δ/Δ MEFs were treated with IR (0.8 Gy) and incubated at 37°C for 30 min. Whole-cell lysates were resolved by SDS-PAGE, transferred to a nitrocellulose membrane, and immunostained with the indicated antibodies.

(B) IF for pATM and NBS1 in IR, or IR and ATM inhibitor-treated HeLa cells transfected with siRNA against ATMIN or control siRNA.

(C) Quantification of the average intensity of pATM foci per cell at the indicated times after IR was performed via a high-throughput Cellomics ArrayScan. At least 300 cells were scored, and values represent the average of three experiments; *$p < 0.05$.

(D) *atmin*F/F and *atmin*ΔG/ΔG mice were irradiated with IR (14 Gy) and sacrificed 2 hr later. Small-intestine tissue lysate was prepared by homogenization in radioimmunoprecipitation assay buffer supplemented with protease and phosphatase inhibitors, and analyzed by SDS-PAGE.

(E) IF of fixed paraffin-embedded intestine tissue showing 53BP1 foci in representative crypts of the indicated genotypes taken at similar time points as for western analysis.

(F) Quantification of 53BP1-positive cells by IHC-IF in *atmin*F/F (n = 5) and *atmin*ΔG/ΔG (n = 6) intestinal crypts; **$p = 0.003$. In all experiments, error bars show the SEM, and Student's t test was used for statistical analysis. In (C) and (F), error bars show the SD of at least three independent experiments.

See also Figure S1.

a C-terminal motif homologous to that of NBS1 (Kanu and Behrens, 2007), raising the possibility that the proteins may interact with the same region of ATM in a mutually exclusive manner. Therefore, we next tested whether increased ATMIN protein levels are able to compete with NBS1 for ATM activation. Indeed, overexpression of ATMIN impaired IR-induced ATM signaling and reduced the levels of pSMC1, pP53, and pKap1 (Figure 2A). Densitometric quantification revealed an inverse correlation between ATMIN protein levels and pATM and pKap1 (Figures S2A and S2B).

ATMIN contains four N-terminal Zn^{2+} fingers, which are predicted to interact with DNA, in addition to the C-terminal ATM interaction motif (Kanu and Behrens, 2007; Figure 2B). In response to IR, overexpression of full-length ATMIN prevented the recruitment of NBS1 to sites of DNA damage marked by γH2AX. Small interfering RNA (siRNA)-mediated depletion of NBS1 abolished NBS1 focus formation, confirming the specificity of the NBS1 IF staining (Figure S2C). Whereas the DNA-binding domain of ATMIN (ATMINΔC) was dispensable, the ATMIN C terminus (ATMINΔN) was both necessary and sufficient for ATMIN competition with NBS1 (Figures 2C and 2D). Western blot analysis showed that overexpression of the ATMIN C terminus impaired ATM-mediated substrate phosphorylation (Figure 2E; quantification of Kap1 phosphorylation is shown in Figure S2D).

NBS1 coimmunoprecipitated with ATM after IR in control-transfected cells, but overexpression of ATMIN reduced the efficiency of the NBS1–ATM interaction and impaired pATM levels and ATM substrate phosphorylation (Figure 2F). Consequently, immunoprecipitation (IP) using a pATM-specific antibody pulled down significantly lower amounts of total ATM protein in ATMIN overexpressing cells. NBS1 was efficiently immunoprecipitated by the pATM antibody, confirming a previous report that NBS1 specifically associates with pATM (Uziel et al., 2003), and ATMIN overexpression also reduced the pATM–NBS1 interaction (Figure 2F). Moreover, concomitant transfection of increasing amounts of NBS1 rescued defective ATM signaling caused by ATMIN overexpression (Figure 2G; quantification of Kap1 phosphorylation is shown in Figure S2E). Thus, ATMIN interferes with IR-induced ATM signaling by competing with NBS1 for ATM

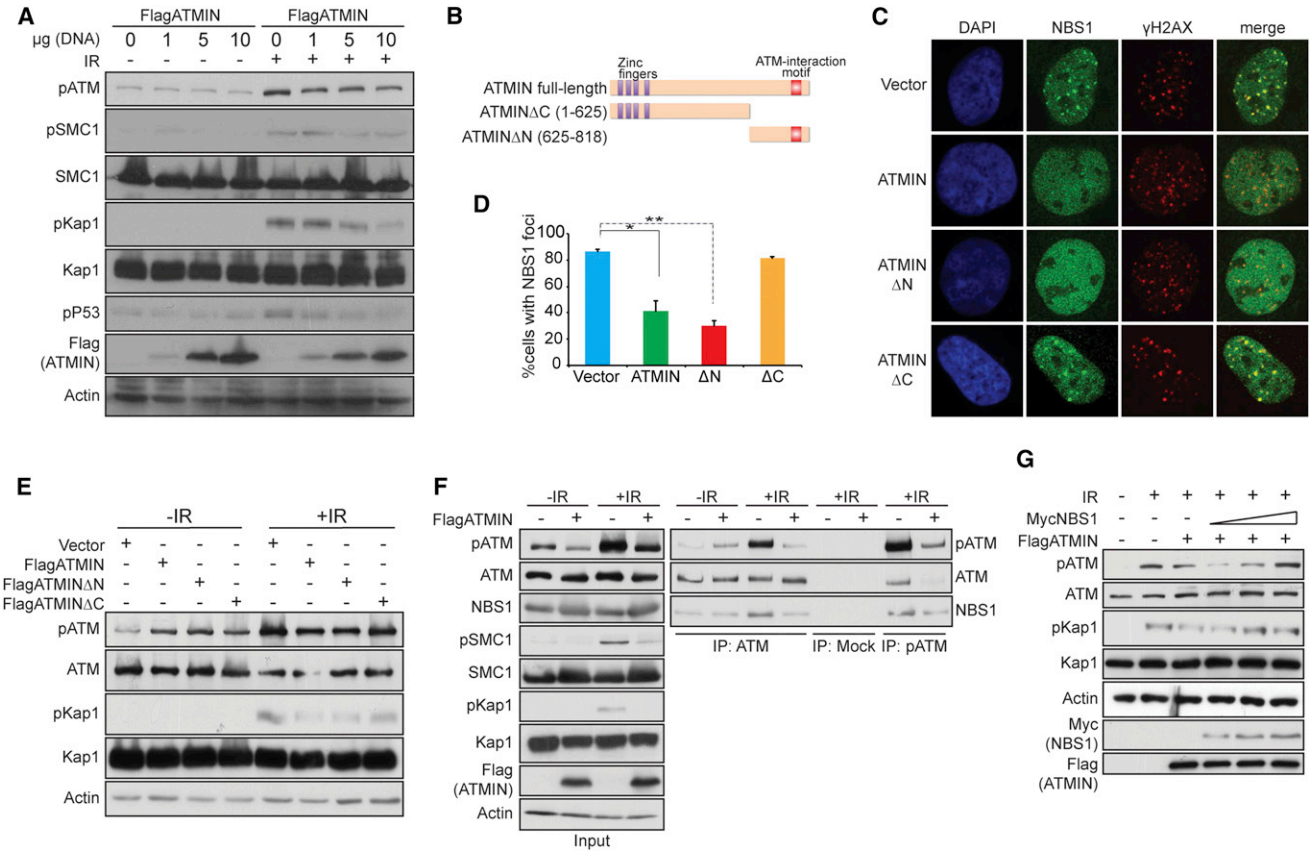

Figure 2. ATMIN Competes with NBS1 for ATM Binding

(A) 293T cells transfected with Flag-ATMIN were treated with IR (2 Gy) and incubated at 37°C for 30 min where indicated. Whole-cell lysates were resolved by SDS-PAGE, transferred to a nitrocellulose membrane, and immunostained with the indicated antibodies.

(B) Schematic of full-length-ATMIN or N/C terminus deletion constructs used in overexpression.

(C) 293A cells transfected with the indicated ATMIN constructs were treated with IR (2 Gy) and immunostained 30 min later with the indicated antibodies.

(D) Quantification of the percentage of NBS1-positive cells by IF; nuclei with at least five NBS1 foci were counted. The graph shows the average of three experiments in which at least 100 cells were scored. Error bars show the SD of at least three independent experiments; Student's t test was used for statistical analysis; *p = 0.01, **p = 0.001.

(E) 293T cells overexpressing the indicated ATMIN constructs were treated with IR (2 Gy), and proteins from cell lysates were analyzed by SDS-PAGE and probed for the indicated antibodies.

(F) 293T cells transfected with full-length Flag-ATMIN were treated with IR (2 Gy), and whole-cell lysate was used to immunoprecipitate ATM, pATM, or control IP.

(G) 293T cells were transfected with equal amounts of full-length Flag-ATMIN and an increasing amount of Myc-NBS1. Cells were treated with IR (2 Gy) and incubated for 30 min prior to lysis.

See also Figure S2.

binding. Because the ATM interaction motifs of the two proteins are similar, and the ATMIN C terminus is sufficient to compete with NBS1, it is likely that the competition is direct, but we cannot rule out contributions from other physical contacts with ATM.

ATMIN Deficiency Rescues Proliferation Arrest and Induction of Senescence in the Absence of NBS1

We next investigated whether the competition between NBS1 and ATMIN would also regulate noncanonical ATMIN-dependent ATM signaling. As expected, NBS1-deficient cells showed dramatically reduced ATM signaling in response to IR. Exposure to hypotonic stress resulted in phosphorylation of p53 in wild-type (WT) cells, which was modestly increased in NBS1-deficient MEFs (Figure 3A, compare lane 6 with lane 3). Thus, although NBS1 is required for IR-induced ATM signaling, the absence of NBS1 appears to increase flux through the ATMIN-dependent arm of the ATM signaling pathway.

To study the significance of increased ATMIN-dependent ATM signaling in *nbs1* mutant cells, we isolated primary MEFs from *nbs1*F/F, *atmin*F/F and compound floxed mice, and acutely inactivated gene function by adenoviral expression of Cre recombinase (Figure S3A). NBS1 is required for proliferation and viability of MEFs under standard culture conditions that involve atmospheric levels of oxygen (20%; Yang et al., 2006). WT MEFs do not undergo cellular senescence at physiological oxygen levels (3%), implying that oxidative damage underlies the senescence of MEFs in culture (Parrinello et al., 2003). When the MEFs were cultured in 3% oxygen, inducible deletion of floxed *nbs1* (yielding

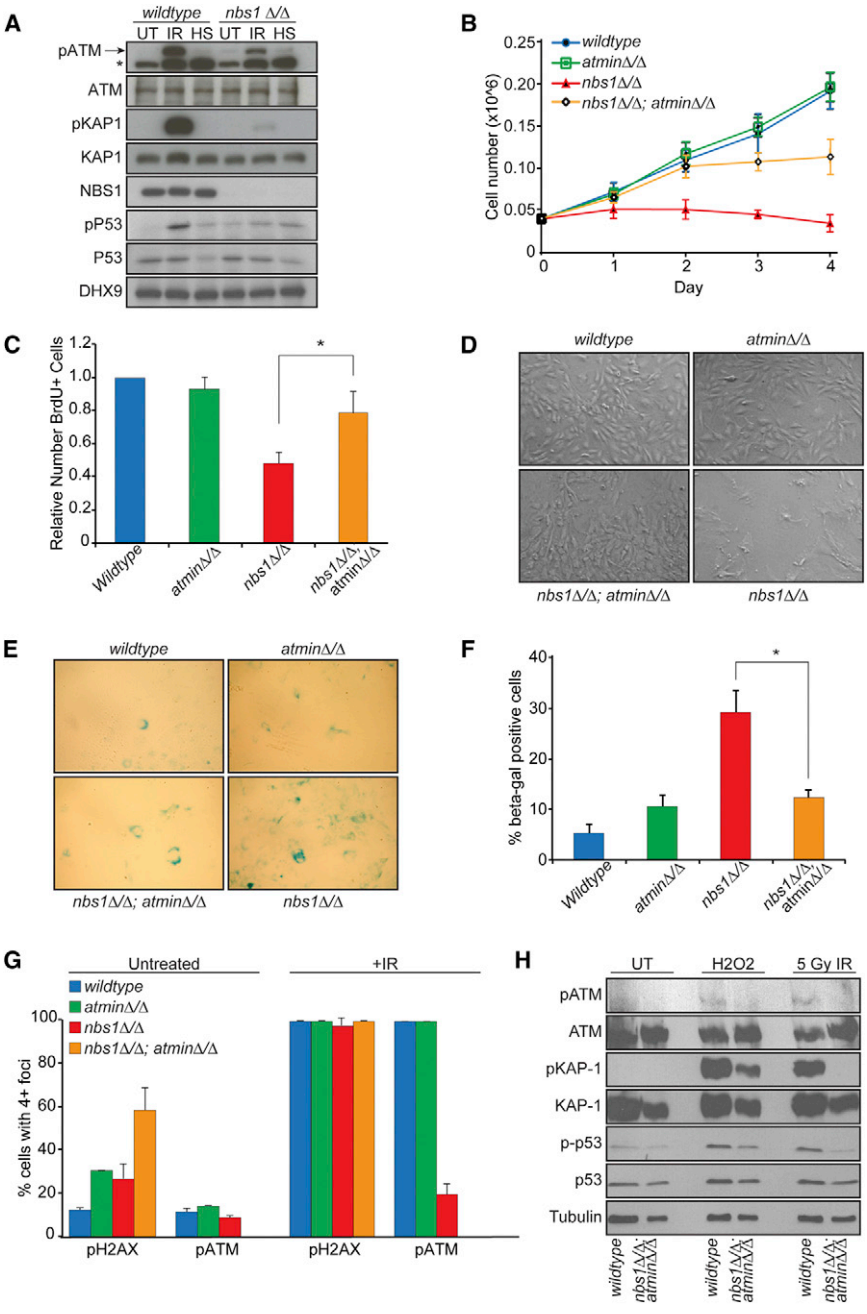

Figure 3. ATMIN Deficiency Rescues Proliferation Arrest and Induction of Senescence in the Absence of NBS1

(A) WT and *nbs1Δ/Δ* MEFs were treated with either 135 mOsm hypotonic shock buffer for 1 hr or 2 Gy IR, and harvested after 15 min. Whole-cell lysates were immunostained with the indicated antibodies; * indicates an unspecific band.

(B) *atmin*$^{f/f}$, *nbs1*$^{f/f}$, and *nbs1*$^{f/f}$;*atmin*$^{f/f}$ MEFs were infected with either AdenoGFP (WT) or AdenoCreGFP (*atminΔ/Δ*, *nbs1Δ/Δ*, and *nbs1Δ/Δ; atminΔ/Δ*). Seven days after infection, 0.04 × 10^6 cells per well were plated and the total cell number was counted in triplicate each day for the next 4 days.

(C) MEFs were cultured in medium containing 10 μM BrdU for 30 min, and the percentage of cells that incorporated BrdU was analyzed by flow cytometry. The percentage of BrdU-positive cells is expressed relative to WT; *p = 0.039.

(D) Representative photographs of the indicated genotypes 10 days after infection of *atmin*$^{f/f}$, *nbs1*$^{f/f}$, and *nbs1*$^{f/f}$;*atmin*$^{f/f}$ MEFs with either AdenoGFP (WT) or AdenoCreGFP (*atminΔ/Δ*, *nbs1Δ/Δ*, and *nbs1Δ/Δ;atminΔ/Δ*).

(E) Ten days after infection, the percentage of senescent cells was analyzed by β-galactosidase staining.

(F) Quantification of (E); *p = 0.0028.

(G) Seven days after AdenoCre-mediated gene deletion, cells were either fixed untreated or fixed 60 min after treatment with 5 Gy irradiation, and then stained for pS1987-ATM and pS139-H2AX. In (B), (C), (F), and (G), error bars show the SD of at least three independent experiments; Student's t test was used for statistical analysis.

(H) MEFs were treated with 5 Gy IR or 250 μM H_2O_2 and lysed after 60 min. Whole-cell lysates were resolved on a 6% SDS-PAGE gel, transferred to a nitrocellulose membrane, and immunostained with the indicated antibodies.

See also Figure S3.

*nbs1*Δ/Δ cells) nevertheless resulted in rapid cessation of proliferation, whereas control and ATMIN-deficient cells proliferated normally and reached confluence. The cumulative cell number reached by *nbs1*Δ/Δ; *atmin*Δ/Δ double-mutant MEFs was increased compared with NBS1-deficient cells, but did not reach WT levels (Figure 3B; Figure S3B). To investigate the defects of NBS1-deficient cells, we measured proliferation by bromodeoxyuridine (BrdU) incorporation. The proliferation of *nbs1*Δ/Δ MEFs was severely impaired, and this defect was partially rescued in double-mutant MEFs (Figure 3C). Moreover, within several days after gene inactivation, a large percentage of *nbs1*Δ/Δ MEFs showed signs of cellular senescence, such as a flat, enlarged morphology and proliferative arrest at subconfluent densities (Figure 3D). Detection of senescence-associated β-galactosidase activity revealed that the *nbs1*Δ/Δ MEFs had entered cellular senescence prematurely. The induction of senescence was ameliorated by *Atmin* deletion in double-mutant cells (Figures 3E and 3F). Whereas *nbs1*Δ/Δ MEFs could only be kept in culture for a few days, *nbs1*Δ/Δ; *atmin*Δ/Δ double-mutant MEFs could be passaged several times; however, the double-mutant MEFs did eventually also undergo premature senescence (data not shown). Thus, ATMIN deficiency ameliorates both the proliferation defect and the premature senescence of *nbs1*Δ/Δ MEFs.

To dissect the relative functional roles of NBS1 and ATMIN in DNA damage signaling and repair, we analyzed spontaneous and IR-induced DNA damage and ATM signaling. Both

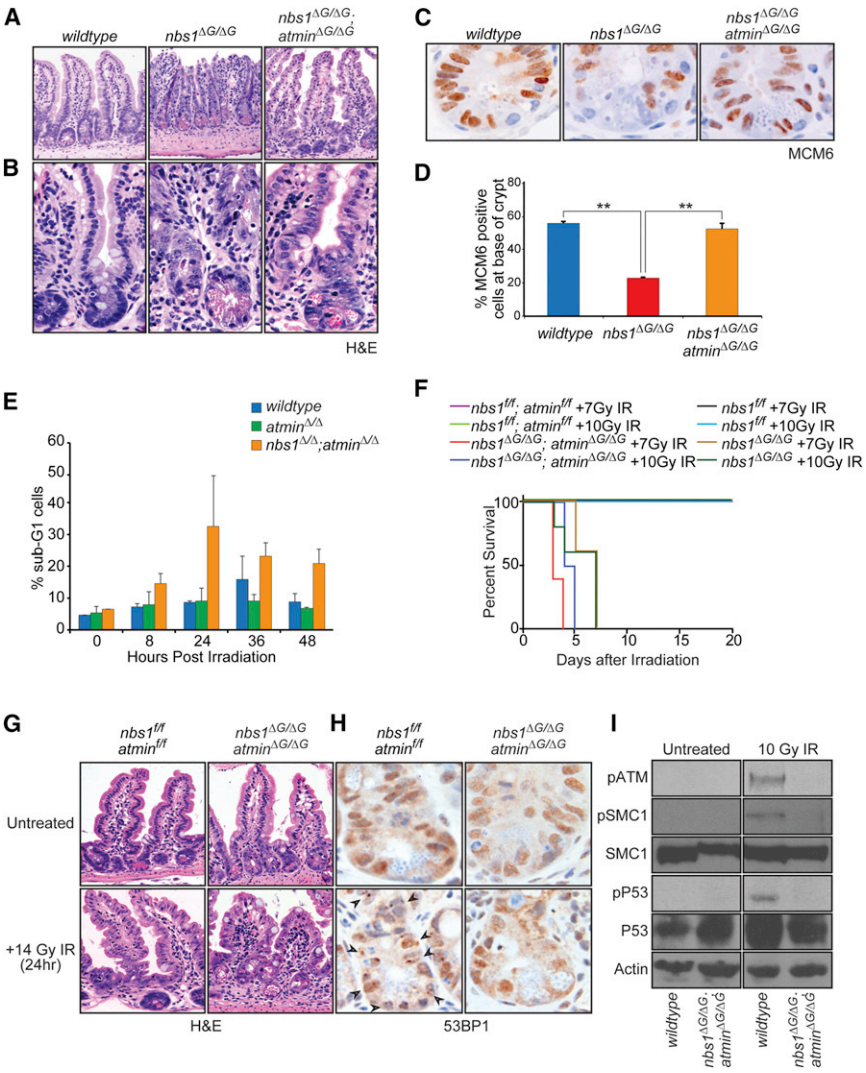

Figure 4. Antagonism and Redundancy of ATMIN and NBS1 for ATM Signaling and Function

(A) H&E staining on representative intestines of mice with the indicated genotypes, 5 days after Villin-creERT-mediated deletion of *Atmin* and *Nbs1*.

(B) High-magnification representation of H&E-stained crypts.

(C) Representative MCM6 IHC on intestines of mice with the indicated genotypes, 5 days after Villin-creERT-mediated deletion of *Atmin* and *Nbs1*.

(D) Quantification of (C); **p = 0.0093.

(E) Cells were treated with 20 Gy irradiation and fixed at the indicated time points post treatment. The percentage of subG1 cells was determined by flow cytometry analysis. In (D) and (E), error bars show the SD of at least three independent experiments, and Student's t test was used for statistical analysis.

(F) Four days after Villin-creERT-mediated deletion of *Atmin* and *Nbs1*, mice were treated with the indicated doses of irradiation (n = 5 mice per genotype per dose).

(G) H&E staining on representative intestines of mice with the indicated genotypes, 24 hr after treatment with 14 Gy irradiation.

(H) Representative 53BP1 IHC in intestines of mice with the indicated genotypes, 24 hr after treatment with 14 Gy irradiation. Arrowheads indicate cells with 53BP1 foci.

(I) Mice were culled 2 hr after 10 Gy irradiation, and protein lysates were prepared from intestinal tissue. Lysates were resolved on a 6% SDS-PAGE gel and the membrane was probed for pS1987-ATM, pS957-SMC1, SMC, pS15-p53, p53, and actin.

See also Figure S4.

*nbs1*Δ/Δ and *atmin*Δ/Δ mutant MEFs showed increased numbers of cells with γH2AX foci, in line with previous observations (Kanu et al., 2010, Yang et al., 2006; Figures 3G and S3C). Spontaneous DNA damage was increased even further in *nbs1*Δ/Δ; *atmin*Δ/Δ double-mutant MEFs, indicating that NBS1 and ATMIN cooperate in the maintenance of genomic integrity. Pharmacological inhibition of DNA-PK substantially reduced γH2AX foci in *nbs1*Δ/Δ; *atmin*Δ/Δ cells (Figure S3D), indicating that DNA-PK is the major γH2AX kinase in double-mutant cells.

Background levels of IF staining for pATM were observed in control, *nbs1*Δ/Δ, and *atmin*Δ/Δ single-mutant MEFs, but pATM was not detectable in *nbs1*Δ/Δ; *atmin*Δ/Δ double-mutant cells (Figures 3G and S3C). Likewise, NBS1/ATMIN double deficiency completely abolished 53BP1 focus formation (Figures S3E–S3G). After IR, NBS1 deficiency led to a substantial decrease in the percentage of cells with pATM foci compared with control cells, but, strikingly, pATM staining was undetectable in double-mutant cells (Figures 3G and S3C). Western blot analysis confirmed that *nbs1*Δ/Δ; *atmin*Δ/Δ MEFs show no detectable IR-induced ATM autophosphorylation or ATM substrate phosphorylation (Figure 3H). Thus, the residual DSB-induced ATM signaling observed in *nbs1*-deficient cells appears to be mediated by ATMIN. Notably, although ATM autophosphorylation was strongly reduced, phosphorylation of ATM substrates still occurred in *nbs1*Δ/Δ; *atmin*Δ/Δ cells in response to oxidative stress (Figure 3H), suggesting the existence of NBS1/ATMIN-independent ATM signaling, possibly via a disulphide-cross-linked dimer (Guo et al., 2010).

Antagonism and Redundancy of ATMIN and NBS1 for ATM Signaling and Function

To study the interplay of ATMIN and NBS1 in more detail, we generated mice lacking NBS1 function in the intestine (tamoxifen-treated *nbs1*F/F; *Villin-creERT* or *nbs1*ΔG/ΔG mice; Figure S4A). Inactivation of NBS1 resulted in a structural disintegration of the intestinal mucosa, but in double-mutant animals the intestinal architecture remained largely intact (Figures 4A and 4B; Figures S1E–S1H). MCM6 is a marker of undifferentiated cells at the bottom of the intestinal crypt (Haigis et al., 2006). *nbs1*ΔG/ΔG mice showed a substantial reduction in MCM6-positive cells, whereas the numbers in *nbs1*ΔG/ΔG;

*atmin*ΔG/ΔG mice were comparable to those in controls (Figures 4C and 4D). Thus, ATMIN inactivation prevents progenitor cell loss induced by NBS1 deficiency.

We next tested the functionality of DNA repair in response to IR in vitro and in vivo. In contrast to WT and *atmin*Δ/Δ MEFs, NBS1/ATMIN double deficiency rendered cells radiosensitive (Figure 4E). Likewise, *atmin*ΔG/ΔG; *nbs1*ΔG/ΔG mice were extremely sensitive to whole-body irradiation and succumbed to low doses (7 and 10 Gy) that were well tolerated by control animals (Figure 4F). Double-mutant mice succumbed more quickly than single-mutant *nbs1*ΔG/ΔG mice, despite the improved structural integrity of the intestine before irradiation. Histologically, the guts of double-mutant mice showed massive radiation injury and cell loss (Figure 4G). In response to very high doses of irradiation, *atmin*ΔG/ΔG; *nbs1*ΔG/ΔG mice showed numerous γH2AX foci (Figure S4B) but complete absence of 53BP1 focus formation (Figure 4H), and no ATM substrate phosphorylation was detectable (Figure 4I). Thus, ATMIN deficiency renders the *nbs1* mutant cellular phenotype similar to the *atm* mutant phenotype.

Although ATMIN deficiency improves the proliferation defect and premature senescence of *nbs1*Δ/Δ MEFs, the rescue is not complete. NBS1 is essential for localization of Mre11 and Rad50 to the nucleus (Williams et al., 2010), and MRN has many biological functions, some of which are likely to be ATM-independent (Dar et al., 2011; Deng et al., 2009; Williams et al., 2010). Consequently, these defects will persist in *nbs1*Δ/Δ; *atmin*Δ/Δ double-mutant cells.

The ATMIN-dependent rescue of *nbs1*Δ/Δ cells occurs despite greatly increased amounts of DNA damage in *nbs1*Δ/Δ; *atmin*Δ/Δ double-mutant cells, indicating that the phenotypes of NBS1-deficient cells cannot be ascribed solely to accumulation of DNA damage per se. The most plausible explanation for our findings is that enhanced ATMIN-dependent ATM signaling underlies the cellular defects of *nbs1*Δ/Δ cells, perhaps by causing activity changes in p53 and other substrates. Thus, the consequences of *nbs1* deficiency for ATM signaling are complex. Both defective DSB-induced ATM signaling and increased ATMIN-dependent ATM signaling appear to contribute to the defects observed in *nbs1* mutant cells. Taken together, our data suggest that the competition between NBS1 and ATMIN for ATM interaction is a fundamental mechanism of ATM signaling, and that disruption of this balance is deleterious to cells.

EXPERIMENTAL PROCEDURES

Cell Culture, Transfection, and Infection

Primary MEF cells were derived from embryonic day 12.5 (E12.5) embryos, and 293 and primary MEF cells were cultured in Dulbecco's modified Eagle's medium supplemented with 10% fetal calf serum (FCS) at 37°C with 5% CO_2 and 3% O_2. For Cre-mediated deletion of floxed alleles, MEF cells were infected with Adeno-Cre-green fluorescent protein (GFP) or Adeno-GFP virus (Gene Transfer Vector Core, Iowa University) for 48 hr. The virus was then removed and the cells were allowed 48 hr to recover before passaging. Transient transfections of 293 cells were performed with Lipofectamine 2000 (Invitrogen) according to the manufacturer's protocol. RNA-induced silencing complex (RISC)-free control siRNA and siRNA SMARTpool against human ATMIN were obtained from Thermofisher. siRNA transfection of 293 cells and HeLa cells was performed using Dharmafect 1 (Invitrogen) and Lullaby reagent (Ozbiosciences), respectively.

IF

Cells were adhered onto slides, treated as indicated in Figures 1B and 2C, and fixed with 4% paraformaldehyde. The cells were permeabilized with 0.5% Triton/PBS and blocked with 10% FCS/PBS/0.1% Triton X-100 before addition of the primary antibody (as indicated in the figures) diluted 1:400 in blocking buffer, pS1981-ATM (10H11.E12; Cell Signaling), pH2AX (07-164; Upstate), NBS1 (NB100-143; Novus Biologicals), and 53BP1 (sc-22760; Santa Cruz). Cells were washed three times with blocking buffer followed by the addition of secondary antibody (Alexa Fluor 568, Alexa Fluor 647, Alexa Fluor 546, and Alexa Fluor 488; Invitrogen), diluted 1:400 in blocking buffer for 1 hr. The cells were washed with PBS and incubated with DAPI before they were mounted in Mowiol (475904; Calbiochem).

Western Blotting

Western blots were performed using standard procedures. Whole-cell lysates were separated by SDS–PAGE and subsequently transferred onto polyvinylidene fluoride membranes (Sancho et al., 2010). The following antibodies were used: pS1981-ATM (10H11.E12; Cell Signaling), ATM (2C1; Santa Cruz), pS824-Kap1 (Bethyl Laboratories), Kap1 (Bethyl Laboratories), β-actin (A5060; Sigma), pS957-SMC1 (5D11G5; Millipore), SMC1 (AB3908; Millipore), pS966-SMC1 (A300-050A; Bethyl Laboratories), p53 (2524; Cell Signaling), NBS1 (NB100-143, Novus Biologicals), DHX9 (gift from Professor F. Grosse), pS15-p53 (9284 and 9286; Cell Signaling), pATM (2152-1, Epitomics), horseradish-peroxidase-conjugated goat anti-mouse/rabbit immunoglobulin G (Jackson). All primary and secondary antibodies were used at 1:1,000 and 1:5,000 dilution, respectively.

IP

For IP, 293T cells were transfected and irradiated prior to lysis for 30 min at 4°C in 500 μl of IP buffer containing 150 mM NaCl, 0.5% Triton X-100, 1 mM EDTA, 100 μM Na-orthovanadate, 0.25 mM phenylmethanesulfonylfluoride, and protease inhibitor mixture (Sigma). After centrifugation, the supernatants were incubated overnight at 4°C with antibody prior to binding of Protein G-Sepharose beads for 3–4 hr. Monoclonal antibodies specific for total ATM (2C1; Santa Cruz), pATM (10H11.E12; Cell Signaling), or isotype-matched control antibody JunB (C11; Santa Cruz) were used.

DNA Damage Treatments and Radiosensitivity Assay

During some experiments, cells were incubated with 10 μM ATM inhibitor (118500; Calbiochem) or 10 μM DNA-PK inhibitor (DNA-PKi) II (260921; Merck Biosciences). For the radiosensitivity assay, cells were treated with 20 Gy IR and fixed in 70% ethanol at the time points indicated in Figure 4E. Fixed cells were stained with Hoechst and analyzed with the use of a FACScan (BD Biosciences). IR experiments were performed using a Cs137 gamma irradiator at 2.1 Gy/min. For hypotonic shock treatment, cells were incubated in hypotonic shock buffer (50 mM NaCl in 1% FBS/PBS supplemented with 0.45% glucose) for 60 min. β-galactosidase-associated senescence staining was performed according to the manufacturer's instructions (Sigma).

Immunohistochemistry

Mice were euthanized by cervical dislocation and the small intestine was prepared for histology as previously described (Sancho et al., 2010). Sections were cut at 4 μm for hematoxylin and eosin (H&E), fast red, and periodic acid-Schiff (PAS)/alcian blue (AB) staining. For immunohistochemistry (IHC) and IF staining on sections, antibodies against 53BP1 (sc-22760; Santa Cruz), pH2AX (07-164; Upstate), MCM6 (sc9843; Santa Cruz), chromogranin A and B (ab8205; Abcam), lysozyme (A0099; Dako), and caspase 3 (AF835; R&D) were used. To quantify the 53BP1-positive cells per crypt, 100 full crypts were scored.

Statistics

Statistical evaluation was performed using Student's unpaired t test. Data are presented as the mean ± SEM, and $p \leq 0.05$ was considered statistically significant.

Mice

atmin$^{F/F}$ and *nbs1*$^{F/F}$ mice have been described previously (Frappart et al., 2005; Loizou et al., 2011). Mice were injected with three consecutive daily

100 μg/g tamoxifen injections. Villin-creERT deletion efficiency and genotyping of mice was determined with a PCR-based assay using primers specific for the floxed exon 4, deleted exon 4, and WT *Atmin* alleles, as well as for the floxed exon 6, deleted exon 6, and WT *Nbs1* alleles. The following primers were used:

Nbs1fF 5′-CAGGGCGACATGAAAGAAAAC-3′
Nbs1fR 5′- AATACAGTGACTCCTGGAGG-3
Nbs1ΔR 5′-ATAAGACAGTCACCACTGCG-3′
Lox6133F 5′-TCAGCATCTTCTCCAGAGAGACAG-3′
Lox6617R 5′-CACATGTGTACAGCACATTCATTG-3′
Lox10252R 5′-CTCAGGGTACACATACTATGCTTGC-3′.

For irradiation experiments, mice were subjected to whole-body exposure to gamma irradiation from a 137Cs source (1.7 Gy/min) and were sacrificed at intervals after exposure as specified in Figures 1D and 4G–4I. The animals were maintained and bred in the Biological Resources Unit of the London Research Institute. All animal experiments were performed in accordance with UK Home Office and institutional guidelines.

SUPPLEMENTAL INFORMATION

Supplemental Information includes four figures and can be found with this article online at http://dx.doi.org/10.1016/j.celrep.2012.11.002.

LICENSING INFORMATION

ACKNOWLEDGMENTS

We thank V. Costanzo for critical reading of the manuscript and members of the Mammalian Genetics Laboratory for input and discussions. Support was provided by the Experimental HistoPathology Unit, High-Throughput Screening Laboratory, Bioinformatics and Biostatistics Unit, Equipment Park, Biological Resources Unit, and FACS Laboratory of the London Research Institute (Cancer Research UK). T.Z. received an NSS-PhD scholarship from A*STAR (Singapore). This work was supported by an ERC grant (281661 ATMINDDR) to A.B. The London Research Institute is funded by Cancer Research UK.

Received: April 26, 2012
Revised: August 14, 2012
Accepted: November 2, 2012
Published: December 6, 2012

REFERENCES

Dar, I., Yosha, G., Elfassy, R., Galron, R., Wang, Z.Q., Shiloh, Y., and Barzilai, A. (2011). Investigation of the functional link between ATM and NBS1 in the DNA damage response in the mouse cerebellum. J. Biol. Chem. *286*, 15361–15376.

Deng, Y., Guo, X., Ferguson, D.O., and Chang, S. (2009). Multiple roles for MRE11 at uncapped telomeres. Nature *460*, 914–918.

Derheimer, F.A., and Kastan, M.B. (2010). Multiple roles of ATM in monitoring and maintaining DNA integrity. FEBS Lett. *584*, 3675–3681.

el Marjou, F., Janssen, K.P., Chang, B.H., Li, M., Hindie, V., Chan, L., Louvard, D., Chambon, P., Metzger, D., and Robine, S. (2004). Tissue-specific and inducible Cre-mediated recombination in the gut epithelium. Genesis *39*, 186–193.

Falck, J., Coates, J., and Jackson, S.P. (2005). Conserved modes of recruitment of ATM, ATR and DNA-PKcs to sites of DNA damage. Nature *434*, 605–611.

Frappart, P.O., Tong, W.M., Demuth, I., Radovanovic, I., Herceg, Z., Aguzzi, A., Digweed, M., and Wang, Z.Q. (2005). An essential function for NBS1 in the prevention of ataxia and cerebellar defects. Nat. Med. *11*, 538–544.

Guo, Z., Kozlov, S., Lavin, M.F., Person, M.D., and Paull, T.T. (2010). ATM activation by oxidative stress. Science *330*, 517–521.

Haigis, K., Sage, J., Glickman, J., Shafer, S., and Jacks, T. (2006). The related retinoblastoma (pRb) and p130 proteins cooperate to regulate homeostasis in the intestinal epithelium. J. Biol. Chem. *281*, 638–647.

Kanu, N., and Behrens, A. (2007). ATMIN defines an NBS1-independent pathway of ATM signalling. EMBO J. *26*, 2933–2941.

Kanu, N., and Behrens, A. (2008). ATMINistrating ATM signalling: regulation of ATM by ATMIN. Cell Cycle *7*, 3483–3486.

Kanu, N., Penicud, K., Hristova, M., Wong, B., Irvine, E., Plattner, F., Raivich, G., and Behrens, A. (2010). The ATM cofactor ATMIN protects against oxidative stress and accumulation of DNA damage in the aging brain. J. Biol. Chem. *285*, 38534–38542.

Lee, J.H., and Paull, T.T. (2007). Activation and regulation of ATM kinase activity in response to DNA double-strand breaks. Oncogene *26*, 7741–7748.

Loizou, J.I., Sancho, R., Kanu, N., Bolland, D.J., Yang, F., Rada, C., Corcoran, A.E., and Behrens, A. (2011). ATMIN is required for maintenance of genomic stability and suppression of B cell lymphoma. Cancer Cell *19*, 587–600.

Lukas, J., Lukas, C., and Bartek, J. (2011). More than just a focus: the chromatin response to DNA damage and its role in genome integrity maintenance. Nat. Cell Biol. *13*, 1161–1169.

McKinnon, P.J. (2004). ATM and ataxia telangiectasia. EMBO Rep. *5*, 772–776.

Parrinello, S., Samper, E., Krtolica, A., Goldstein, J., Melov, S., and Campisi, J. (2003). Oxygen sensitivity severely limits the replicative lifespan of murine fibroblasts. Nat. Cell Biol. *5*, 741–747.

Sancho, R., Jandke, A., Davis, H., Diefenbacher, M.E., Tomlinson, I., and Behrens, A. (2010). F-box and WD repeat domain-containing 7 regulates intestinal cell lineage commitment and is a haploinsufficient tumor suppressor. Gastroenterology *139*, 929–941.

Savitsky, K., Sfez, S., Tagle, D.A., Ziv, Y., Sartiel, A., Collins, F.S., Shiloh, Y., and Rotman, G. (1995). The complete sequence of the coding region of the ATM gene reveals similarity to cell cycle regulators in different species. Hum. Mol. Genet. *4*, 2025–2032.

Uziel, T., Lerenthal, Y., Moyal, L., Andegeko, Y., Mittelman, L., and Shiloh, Y. (2003). Requirement of the MRN complex for ATM activation by DNA damage. EMBO J. *22*, 5612–5621.

Williams, G.J., Lees-Miller, S.P., and Tainer, J.A. (2010). Mre11-Rad50-Nbs1 conformations and the control of sensing, signaling, and effector responses at DNA double-strand breaks. DNA Repair (Amst.) *9*, 1299–1306.

Yang, Y.G., Saidi, A., Frappart, P.O., Min, W., Barrucand, C., Dumon-Jones, V., Michelon, J., Herceg, Z., and Wang, Z.Q. (2006). Conditional deletion of Nbs1 in murine cells reveals its role in branching repair pathways of DNA double-strand breaks. EMBO J. *25*, 5527–5538.